Available online at www.sciencedirect.com
SCIENCE DIRECT®
Nuclear Instruments and Methods in Physics Research A 545 (2005) 803–812
NUCLEAR INSTRUMENTS & METHODS IN PHYSICS RESEARCH Section A
www.elsevier.com/locate/nima

An improved weighting algorithm to achieve software compensation in a fine grained LAr calorimeter

C. Issever[a,*], K. Borras[b], D. Wegener[c]

[a]*University of Oxford, Particle Physics, Keble Road, Oxford, OX1 3RH, UK*
[b]*DESY, Notkestrasse 85, 22607 Hamburg, Germany*
[c]*University of Dortmund, Otto-Hahn-Strasse 4, 44227 Dortmund, Germany*

Received 3 January 2005; received in revised form 30 January 2005; accepted 8 February 2005
Available online 8 April 2005

Abstract

An improved weighting algorithm applied to hadron showers has been developed for a fine grained LAr calorimeter. In contrast to standard weighting procedures, the new algorithm allows to reconstruct the total energy as well as the spatial energy deposition on the level of individual calorimeter cells. The linearity and the energy resolution of the pion signal in the momentum interval $2\,\mathrm{GeV/c} \leqslant p \leqslant 20\,\mathrm{GeV/c}$ studied in this analysis are considerably improved in comparison to the standard weighting algorithm as practiced presently by the H1 collaboration. Moreover the energy spectra reconstructed with the new method follow in a broad interval a Gaussian distribution and have less pronounced tails.

PACS: 07.20.Fw

Keywords: Calorimeter; LAr; Software compensation; Energy reconstruction

1. Introduction

The different response of hadron calorimeters to electromagnetic and hadronic showers, observed for the first generation of hadron calorimeters [1–3], are a source of non-linearities, deviations of the relative resolution from the statistically expected $1/\sqrt{E}$ -behaviour and the origin of the non-Gaussian shape of the response function [4,5]. Two different methods have been proposed to avoid these disadvantages. Hardware compensation, optimized by extensive simulations of hadron showers [5–7], enhances the hadron signal by detecting neutrons, produced in hadron ^{238}U interactions, with scintillators [8,9]. On the other hand, in fine grained calorimeters the signal of different detector cells can be weighted in such a

*Corresponding author. Tel.: +44 1865 273410; fax: +44 1865 273417.
E-mail address: c.issever1@physics.ox.ac.uk (C. Issever).

0168-9002/$ - see front matter © 2005 Elsevier B.V. All rights reserved.
doi:10.1016/j.nima.2005.02.010

way that the overall signal of electrons and hadrons depositing the same energy is equalized. This method was pioneered by the CDHS Collaboration [4] using a large scintillator-iron calorimeter to detect hadron showers produced in ν-events. Essential improvements were achieved by the H1 Collaboration [10–13] exploiting the high granularity of its 45 000 channel LAr calorimeter.

In this paper, a new weighting algorithm is presented which not only allows to determine the deposited energy in an improved way but in addition permits a more realistic reconstruction of the spatial shower distribution. While previous algorithms aimed just for a determination of the total shower energy, the new method intends to reconstruct the energy in each cell of the calorimeter hit by the hadronic shower. Losses due to noise suppression cuts applied to individual cells are considered separately by adding a correction term to the total reconstructed energy.

After a short description how the visible energy is derived from the measured charge, which is identical to the standard procedure of the H1 algorithm [14,16,17], the new method is explained. The weights, and the measurable variables they depend on, are determined next, followed by a description of the algorithm, correcting for losses due to noise. Finally, the new weighting algorithm is applied to Monte Carlo and test beam data. The results achieved are compared to those of the standard H1 algorithm described in Refs. [14,16,17].

2. Reconstruction of the visible energy

2.1. Determination of the electromagnetic calibration constant

The electromagnetic calibration constant which allows to convert the recorded charge into visible energy, has been derived by an iterative procedure [18] equalizing the reconstructed energy of test beam and simulated data for electrons:

$$\langle E_0^{\mathrm{exp}} \rangle = \langle E_0^{\mathrm{sim}} \rangle. \tag{1}$$

The experimentally determined energy is derived from the deposited charges Q_i

$$\langle E_0^{\mathrm{exp}} \rangle = C_{\mathrm{exp}} \left\langle \sum_i Q_i \right\rangle \tag{2}$$

where the sum runs over all calorimeter cells with a signal passing the noise cuts. The reconstructed signal of simulated data is given by the expression

$$\langle E_0^{\mathrm{sim}} \rangle = \left\langle \sum_i (C_{\mathrm{sim}} E_{\mathrm{vis}}^i + C_{\mathrm{exp}} Q_{\mathrm{noise}}^i) \right\rangle \tag{3}$$

$$C_{\mathrm{sim}} = \left\langle \frac{E_{\mathrm{dep}}}{E_{\mathrm{vis}}} \right\rangle \tag{4}$$

where C_{sim} is derived from simulated data. E_{dep} is the energy deposited in the calorimeter, while

$$E_{\mathrm{vis}} = \sum_i E_{\mathrm{vis}}^i \tag{5}$$

is the detected visible energy in the active medium of the calorimeter derived by simulation. The influence of saturation phenomena, charge losses due to electron capture by electronegative gases [19], recombination in the ionization column [20], etc. were derived from HV curves recorded before and after the data collection. In addition, probes similar to those used finally in the H1 calorimeter [21] monitored the response to the signal of a radioactive source continuously. Q_{noise}^i is the measured noise in calorimeter channel i. C_{exp} is obtained iteratively from Eqs. (2)–(4) requiring the constraint (1) to hold for electrons.

The calibration constant C_{exp} determined by this method defines the electromagnetic scale of the calorimeter. The reconstructed energy E_0^i of cell i on the electromagnetic scale for test beam data is given by the expression

$$E_0^i = C_{\mathrm{exp}} Q_i \tag{6}$$

and for simulated data by

$$E_0^i = C_{\mathrm{sim}} E_{\mathrm{vis}}^i + C_{\mathrm{exp}} Q_{\mathrm{noise}}^i \tag{7}$$

in analogy to Eqs. (2) and (3).

The data used in the present analysis were collected at the CERN SPS test beam H6 [22] using a FB2-type module of the H1 LAr calorimeter [23,24]. The simulation employed the H1

software packages H1SIM [25] and ARCET [26] based on the event generators GEANT 3.21 [27] and GHEISHA [28].

2.2. Clustering of energy

The identification of calorimeter cells hit by the hadron showers follows the standard methods developed by the H1 Collaboration, described in more detail in Refs. [14,15,17]. Besides, the charge produced by the hadron shower electronic noise contributes to the detected signal which amounts typically to $\sigma_{\text{noise}} = 15\,\text{MeV}$ up to 30 MeV per channel [24]. Only charges with

$$|Q_i| > 2.5\sigma^i_{\text{noise}} \tag{8}$$

are recorded for the calorimeter modules used in the present analysis. In the analysis however an additional cut is applied. Besides those channels with

$$|Q_i| \geqslant 4\sigma^i_{\text{noise}} \tag{9}$$

in addition cells are taken into account which are direct neighbours of a channel with $Q_i > 4\sigma^i_{\text{noise}}$:

$$Q_i > 4\sigma_i \wedge |Q_j| > 2.5\sigma_j \quad \text{with } j = \text{neighbour cell of } i. \tag{10}$$

Clusters combining those cells which pass the noise cuts (8), (9) and (10) are constructed in two steps [14]. First all cells in a given plane of the calorimeter at constant distance from the beam are grouped into 2D-clusters around the cell with the highest charge deposit. In the second step, adjacent 2D-clusters are combined to a 3D-cluster. The topological nearest cells to a 3D-cluster with a negative signal are added to the original cluster. If the total charge of this combination is negative, the 3D-cluster is excluded from the following analysis.

Clusters due to primary photons and electrons are identified by estimators which exploit the characteristic shape of an electromagnetic shower [15,16]. They are not considered further in the analysis. The remaining clusters are labelled as hadronic clusters, all weights are derived from and applied to this subset of the data.

The quantity E_{cone}, the energy deposited inside a cone whose axis connects the interaction vertex with the most significant hadronic cluster, where its significance is defined by

$$p = \sqrt{\sum_i \left(\frac{E^i_0}{\sigma^i_{\text{noise}}}\right)^2} \tag{11}$$

turns out to be an important input variable for the weighting algorithm developed in this paper. E_{cone} is determined in two steps following essentially the procedure developed for the H1 standard analysis [16]. If no other cluster apart from the one defining the cone axis is found within an opening angle of 11° the energy of the cone is given by

$$E_{\text{cone}} = E_{\text{cluster}}. \tag{12}$$

However, if more than one cluster is recorded within this cone, a new one of 11° opening angle is constructed whose axis connects the interaction vertex with the energy centre of gravity of the hadron clusters of the previous cone. In this case, the cone energy is defined by the sum over all clusters in the new cone

$$E_{\text{cone}} = \sum_j E^j_{\text{cluster}}. \tag{13}$$

In the following, the cone reconstructed with the largest energy is referred to as "most energetic cone"; $E^{\max}_{\text{cone}}$ denotes its energy. Further cones are constructed from the remaining hadron clusters following the procedure described above.

2.3. Description of the new weighting algorithm

Two components of the hadron showers strongly influence the energy deposition and the possibilities to measure its energy. The break up of nuclei strongly reduces the detectable energy [5–7]; the lost energy is referred to as "invisible energy" in the following, it has to be compensated by weighting. On the other hand, the electromagnetic component in a hadron shower is deposited in the calorimeter without losses and therefore has not to be weighted.

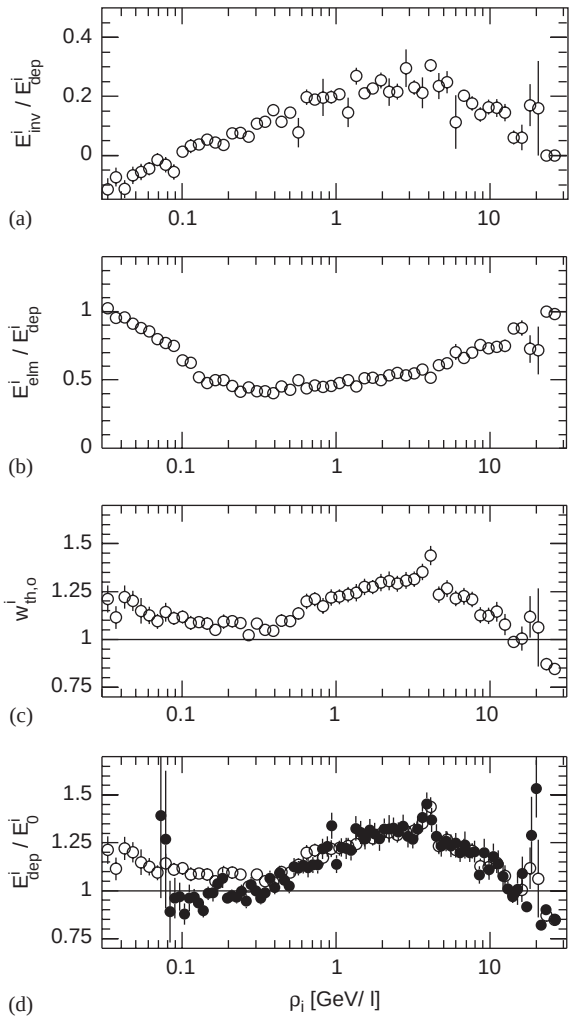

Fig. 1. Fraction of energy deposited in cell i normalized to the corresponding reconstructed energy as function of the energy density ρ_i: (a) invisible energy, (b) electromagnetic energy. Theoretical weights $w^i_{th,0}$ according to Eq. (15) are plotted as a function of ρ_i in (c) and are compared to the weights w^i_{th} (full points) of Eq. (16) in (d). The energy of the primary hadron is 15 GeV.

The energy density

$$\rho_i = \frac{E^i_0}{\mathrm{Vol}^i} \tag{14}$$

in cell i with volume Vol^i allows to tag these components [4].

In Figs. 1a and b the fractional contribution of the invisible energy and the electromagnetic energy to the total deposited energy in cell i, respectively, are plotted as functions of the energy density ρ_i. The electromagnetic component rises with increasing energy density. This behaviour can be traced back to the fact that electromagnetic subshowers have a smaller spatial extension than hadron-induced subshowers.

In Fig. 1c the theoretical weights

$$w^i_{th,0} = \frac{E^i_{dep}}{C_{sim} E^i_{vis}} \tag{15}$$

which according to Eq. (7) do not consider the noise contribution are shown as a function of ρ_i. It reveals a strong variation with ρ_i resulting from the individual dependencies of the invisible and the electromagnetic component on the energy density. $w^i_{th,0}$ is compared in Fig. 1d to the weight

$$w^i_{th} = \frac{E^i_{dep}}{E^i_0} \tag{16}$$

which allows to convert the reconstructed energy E^i_0 of Eq. (7) on the electromagnetic scale into the real deposited energy E^i_{dep}. The differences w^i_{th} and $w^i_{th,0}$ at small energy densities ρ_i can be explained qualitatively as a consequence of the overlayed noise and the noise cuts applied [30].

The theoretical weights $w^i_{th,0}$ in the interval $3\,\mathrm{GeV/l} \leqslant \rho_i \leqslant 30\,\mathrm{GeV/l}$ decrease (Fig. 1c), since in this region the relative contribution of nuclear binding energy diminishes (Fig. 1a), i.e. less energy has to be corrected for. In the interval $0.2\,\mathrm{GeV/l} \leqslant \rho_i \leqslant 3\,\mathrm{GeV/l}$ the theoretical weights $w^i_{th,0}$ increase with ρ_i, this can be attributed to the growth of the invisible energy (Fig. 1a). Especially at lower values of ρ_i the energy of charged particles is deposited by excitation and ionization of atoms; hence contributions from nuclear reactions can be neglected. In the interval $\rho_i < 0.2\,\mathrm{GeV/l}$ the weight $w^i_{th,0}$ increases with decreasing ρ_i. Since these energy densities are characteristic for energy depositions of low-energy electrons and photons in the tail of the shower (see increase of the fractional contribution of the electromagnetic energy in Fig. 1b), the transition effect [5,7,31] reduces the signal and therefore forces the weights to increase.

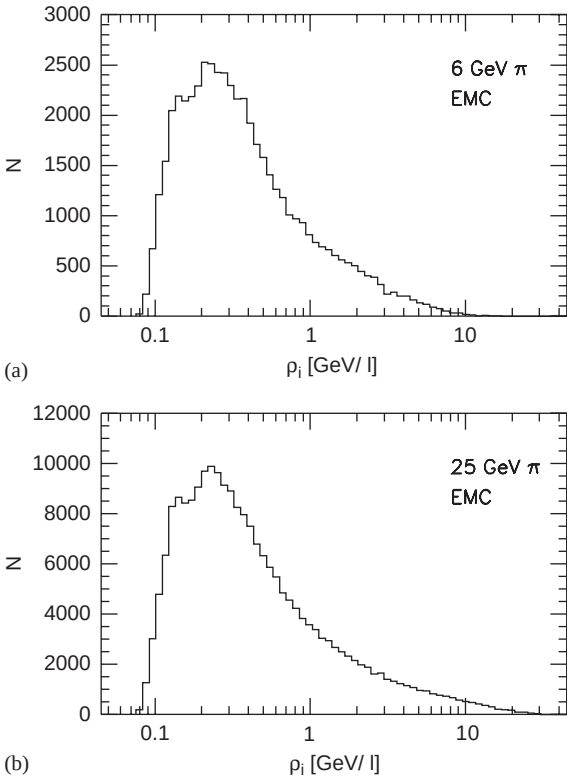

Fig. 2. Distribution of energy density of cells in the "most energetic cone" for pions of (a) 6 GeV/c and (b) 25 GeV/c.

Fig. 2 demonstrates that in first approximation the shape of the energy density distribution is independent of the energy of the primary pion, but a closer look reveals differences especially at large values of ρ_i. This can be attributed to the increase of the electromagnetic fraction in hadron showers at higher primary energies [29]. This effect has to be taken into account in a global way; the energy E_{cone} of the cone provides the necessary information to estimate the initial hadron energy [30] as will be demonstrated.

Hence, the weighting factors of the new algorithm are parameterized as functions of ρ_i and E_{cone}

$$w^i_{\text{new}}(\rho_i, E_{\text{cone}}) = \left.\frac{\langle E^i_{\text{dep}}\rangle}{\langle E^i_0\rangle}\right|_{\rho_i, E_{\text{cone}}}. \quad (17)$$

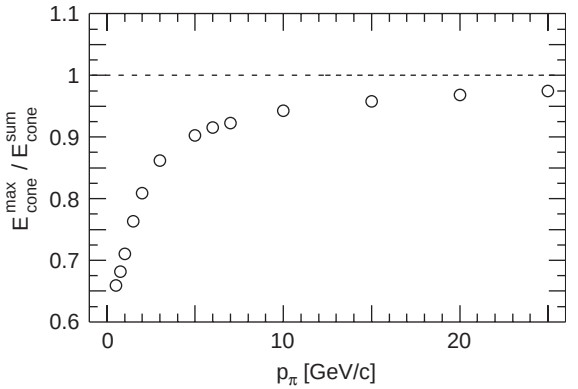

Fig. 3. Fraction of energy reconstructed in the "most energetic cone" normalized to the total reconstructed energy.

They are derived from simulated data taking noise into account and applying noise cuts. $\langle E^i_{\text{dep}}\rangle$ and $\langle E^i_0\rangle$ are the mean values of the deposited and reconstructed energy in a $\rho_i - E_{\text{cone}}$ interval, respectively. Only cells of the "most energetic cone" of an event are considered, since $E^{\max}_{\text{cone}}$ is a convenient measure of the hadron energy initiating the shower. This becomes evident from Fig. 3 where the fraction of energy deposited in the "most energetic cone" is plotted as a function of the primary hadron energy. For $p_\pi > 2\,\text{GeV/c}$ more than 75% of the total reconstructable energy is detected in this cone, this fraction rises strongly with increasing p_π and saturates at ~95%. Hence, for the construction of the weights the choice of $E^{\max}_{\text{cone}}$ as the second variable, on which w^i_{new} depends, makes sense. If the weights of cells for cases with $E_{\text{cone}} < E^{\max}_{\text{cone}}$ would have been considered in addition, corrections for showers with low- and high-deposited energy would be mixed up, while considering only the "most energetic cone" provides clean conditions with small overlap of low- and high-energy data (Fig. 4).

The weights according to Eq. (17) of the new algorithm for the electromagnetic and hadronic modules of the H1-LAr calorimeter in the test set-up are collected in Figs. 5a and b. A double logarithmic scale has been chosen to depict the strong variation of w^i_{new} at small ρ_i, E_{cone} [30]. The new weighting algorithm allocates for each cell i according to its energy density and the energy

of its assigned cone the weighting factor $w^i_{\text{new}}(\rho_i, E_{\text{cone}})$ from the tables shown in Fig. 5. It reconstructs the energy on the hadronic scale E^i_{rec} by multiplying the energy on the electromagnetic scale E^i_0 with the new weight

$$E^i_{\text{rec}} = E^i_0 w^i_{\text{new}}(\rho_i, E_{\text{cone}}). \quad (18)$$

Note that the reconstruction of the energy on the hadronic scale of cells, which do not belong to the most energetic cone, is also performed with the weighting factor shown in Fig. 5.

The application of the new weighting algorithm allows to reconstruct the deposited energy on the cell level. This is demonstrated by Fig. 6, where the

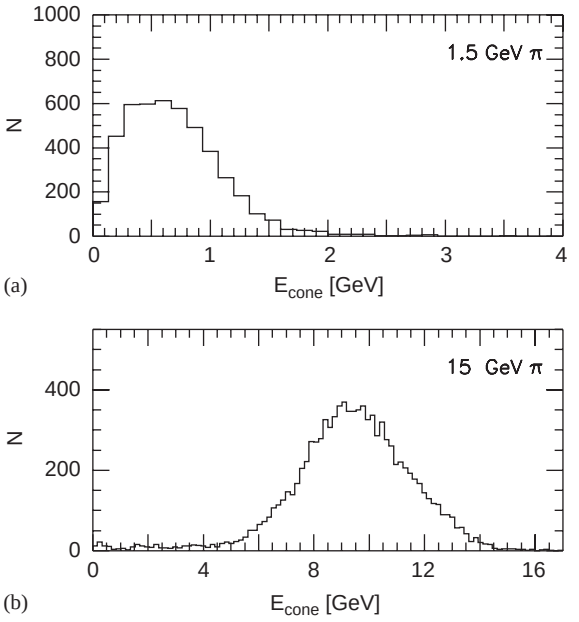

Fig. 4. Distribution of reconstructed energy in the "most energetic cone" (a) for low and (b) for high momentum pions.

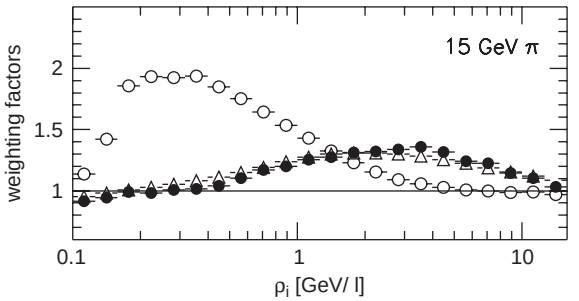

Fig. 6. Comparison of the theoretical weights (full circle) according to Eq. (16) with the new (open triangle) and the H1 standard weights (open circle) as function of the energy density in a cell for 15 GeV pions.

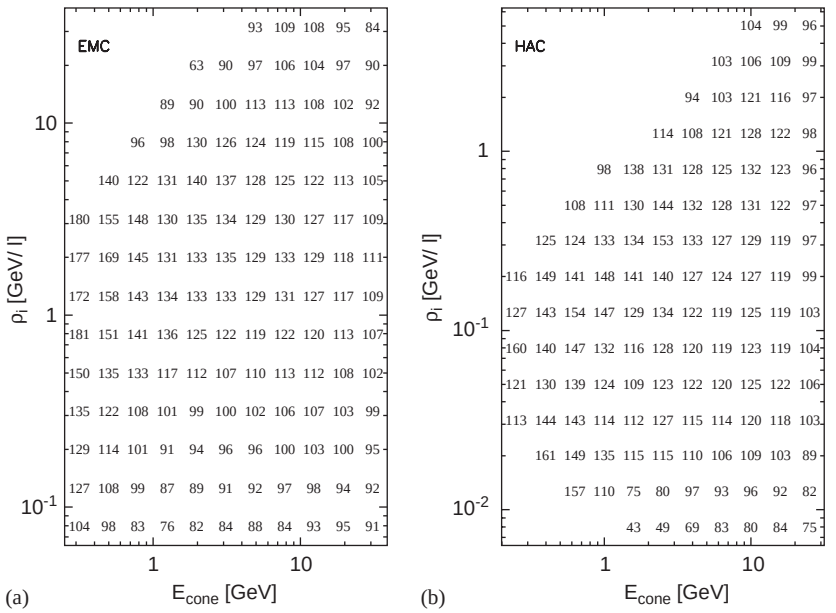

Fig. 5. Weighting factors in percent (a) for the electromagnetic and (b) the hadronic FB2-modules of the H1-LAr test calorimeter set-up [22] as function of the energy in the "most energetic cone" and the energy density in cell *i*.

theoretical weights w^i_{th} of (Eq. (16)) are compared to the applied weights of the H1 standard and of the new algorithm as described in this paper. While the theoretical (full circles) and the applied weights of the new algorithm (open triangle) coincide in good approximation for all values of ρ_i, the H1 standard weights (open circles) differ in their trend from the expectation. Note however that by construction the total energy deposited in the calorimeter is successfully reconstructed by both algorithms. The standard H1 weighting procedure achieves this through the iterative application of weighting functions according to equation:

$$E^i_{\text{rec}} = C_1 \exp(-C_2(E^i_0/\text{Vol}^i)) + C_{3_{\text{EMC/HAC}}} E^i_0,$$

where C_i are parameter functions, which are depending on the jet energy and polar angle of the jet [12]. These weighting and parameter functions have been determined in an iterative process optimizing both the reconstruction of the total energy deposited in the hadronic shower and the resolution. In this iterative process no emphasis is put on the reconstruction of the deposited energy on the level of single cells. For jet energies below 7 GeV the standard H1 weighting procedure replaces the iterative weighting functions by an average e/π correction factor. In the transition region between 7 and 10 GeV the standard H1 weighting procedure interpolates between the average e/π correction factor and the iterative weighting functions.

2.4. Correction of energy losses due to noise cuts

Only those cells can be considered by the weighting algorithm which have a finite signal after the noise cuts, i.e. the new weights derived only optimize the energy reconstruction for cells with a signal above the noise cuts. Hence the losses due to this cut have to be taken into account in a separate step. In contrast to this procedure in the H1 standard analysis the noise correction is included in the weighting factor.

In the new algorithm a first-order approximation noise correction is derived using information of cells belonging to the "most energetic cone". All cells of this cone are considered including those which do not belong to a hadronic cluster. From simulated data including detector noise the total energy deposited in the cone, $E^{\text{dep,tot}}_{\text{cone}}$, and the deposited energy of cells passing the noise cut $E^{\text{dep,rem}}_{\text{cone}}$ are calculated. The correction is given by the expression

$$\Delta E^{\text{dep,cor}}_{\text{cone}} = E^{\text{dep,tot}}_{\text{cone}} - E^{\text{dep,rem}}_{\text{cone}}. \tag{19}$$

The energy correction is evaluated as a function of

$$E^{\text{all}}_{\text{cone}} = \sum_j E^j_{\text{rec}} \tag{20}$$

on the electromagnetic scale, where the sum runs over all cells in the "most energetic cone". It is added to the weighted energy of the cone. The result is shown in Fig. 7. The weak energy dependence for $E^{\text{all}}_{\text{cone}} \leqslant 1$ GeV is due to the fact that in cones with small energy the fractional noise contribution is large hence the signal loss due to the noise cuts is small. With increasing $E^{\text{all}}_{\text{cone}}$, i.e. increasing shower energy, more cells in the cone have a signal which can be suppressed by the noise cut, hence the influence of the noise cuts grows.

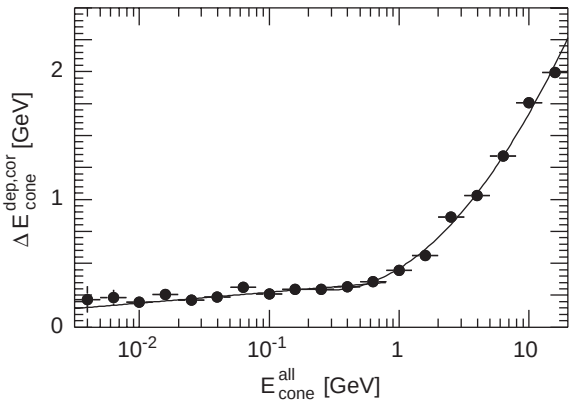

Fig. 7. Correction defined in Eq. (19) considering the losses due to the noise cuts as a function of the sum of all cells in the "most energetic cone".

3. Comparison with simulation and test beam data

The new algorithm is applied to a set of simulated data. The geometry of the simulation

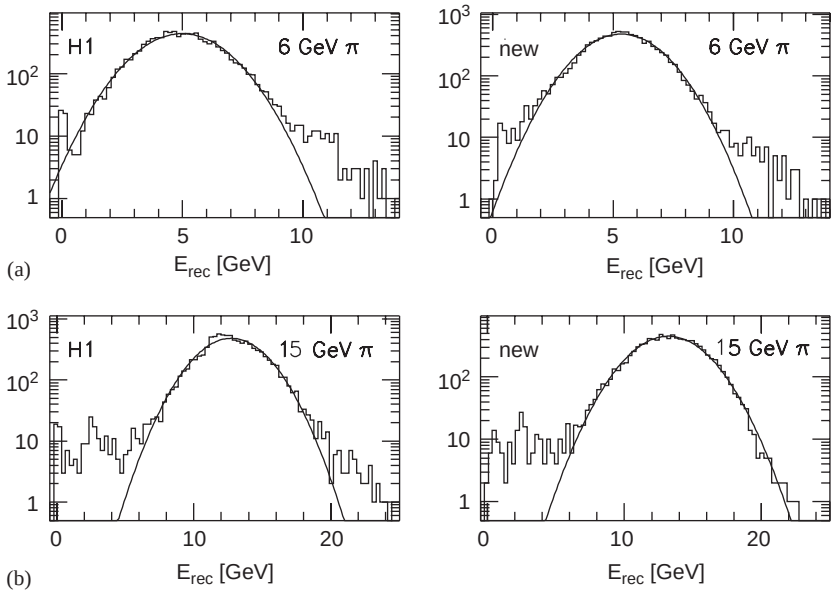

Fig. 8. Comparison of the reconstructed energy distributions (a) applying the standard H1 (left row) and (b) the new weights (right row) for π-mesons of two energies of the primary pion (Monte Carlo simulation).

corresponds to the CERN test beam configuration [22] with an impact angle $\theta = 33.73^{\circ}$ of the primary pion. Also, the geometry of the detector and the cryostat are adapted to the CERN test set-up [22].

Typical distributions of the reconstructed energy are shown in Fig. 8a for the standard H1 and the new improved algorithm (Fig. 8b). For both weighting procedures, a Gaussian shape of the energy distribution is achieved in the peak region. For the new algorithm the tails are smaller, especially at higher beam energies, the high-energy tail is strongly suppressed. Note that energy losses due to material in front of the calorimeter are not corrected for, hence the reconstructed and the primary energy differ.

The energy response is linear within 2% for energies above 2 GeV if one uses the new algorithm while for the standard H1 procedure larger deviation from linearity are observed (Fig. 9). An even better linearity, especially in the region of 5 GeV, would be achievable when using a finer grid in the Monte Carlo simulations for the determination of the new weighting factors. The use of the new algorithm furthermore leads to an improved energy resolution of the calorimeter (Fig. 10).

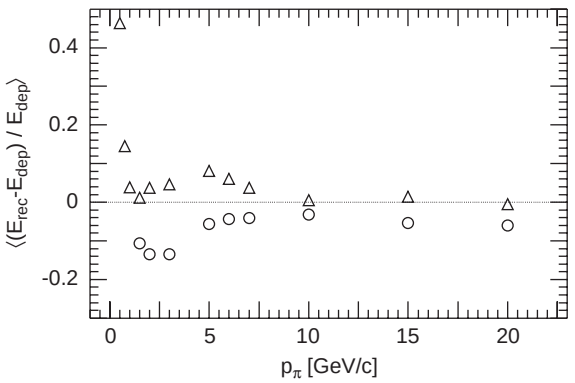

Fig. 9. Difference between reconstructed and deposited energy normalized to the deposited energy as function of the momentum of the primary pion for the H1 standard (open circle) and the new weights (triangle) (Monte Carlo simulation). The Gaussian fits to the reconstructed energy distributions for 0.5, 0.75 and 1 GeV failed for the H1 standard algorithm and hence are not included in the figure.

Finally, the new algorithm also was applied to real data taken at the CERN SPS test beam H6 with a pion beam energy of 20 GeV. In Fig. 11, the

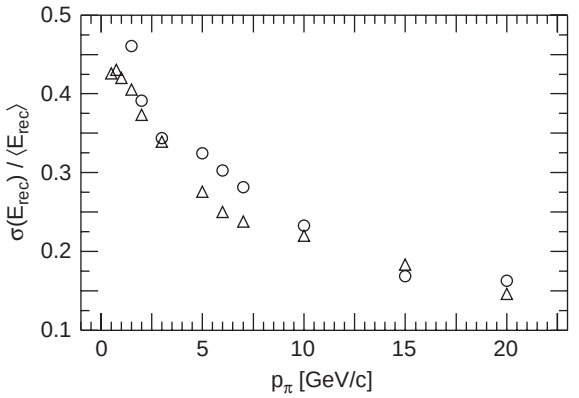

Fig. 10. Relative energy resolution of the reconstructed energies for H1 standard (circles) and for new weights (triangles) (Monte Carlo simulation). The Gaussian fits to the reconstructed energy distributions for 0.5, 0.75 and 1 GeV failed for the H1 standard algorithm and hence are not included in the figure.

reconstructed energy distribution for the two algorithms are compared, again showing an improvement when using the new weights confirming the results from the study of simulated data.

4. Conclusion

A new weighting algorithm has been developed to correct the different response of the H1-LAr calorimeter to electromagnetic and hadronic showers. The essential difference between the new and the standard H1 algorithm consists in the separate treatment of weight factors and the corrections for noise cuts. This separation allows to reconstruct the energy deposited in the cells of the calorimeter properly. Hence, the new algorithm described in this paper not only improves the linearity and the energy resolution (Figs. 9, 10) but in contrast to the H1 standard algorithm it allows to reproduce the shower shape (Fig. 6).

Recently this algorithm has been generalized by Marks [32] in such a way that it can be applied to all modules of the H1-LAr calorimeter at the HERA ep storage ring. Moreover, improved corrections for the noise cuts were developed and the energy range of the new weighting algorithm

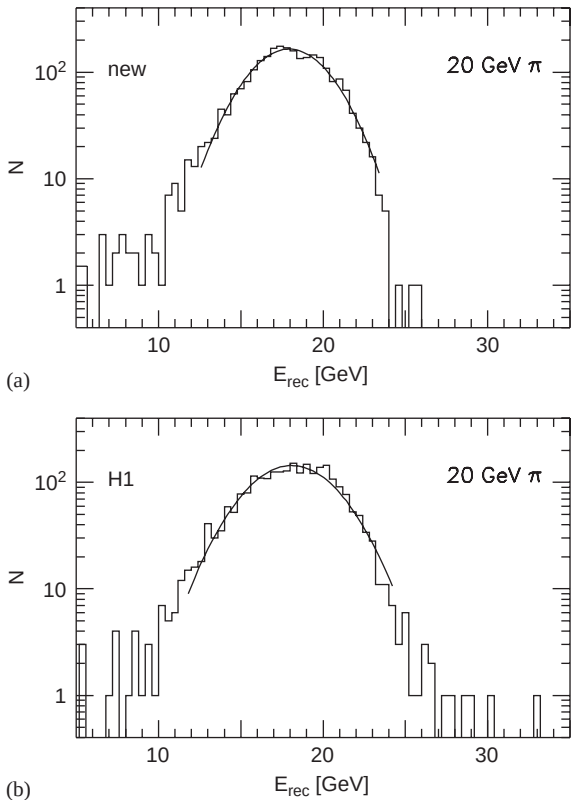

Fig. 11. Distribution of reconstructed energies for test beam data collected at the CERN test beam H6, data were collected with test modules of the H1-LAr calorimeter: reconstructed (a) with new and (b) with H1 standard weights.

was extended. First applications on jets of up to $E_{\text{jet}} = 120\,\text{GeV}$ from a high Q^2 neutral current deep inelastic scattering sample show that the resolution of the balance in transverse momentum between hadronic system and the electron is improved [33]. This new weighting algorithm is particularly important for high granularity calorimeters such as the ATLAS and CMS calorimeters and the calorimetry being developed for the International Linear Collider [34].

Acknowledgements

This work is based on the untiring work of many members of the H1 calorimeter group in the years 1986–1996 to develop a calibration proce-

dure and a version of the weighting algorithm which successfully was applied in the last 10 years by the H1 Collaboration in their data analysis. Special thanks are due to Drs. J. Gayler, P. Loch and J. Spiekermann for stimulating discussions and for help and advice and Dr. H.-C. Schultz-Coulon for careful and critical reading of the manuscript. This work was supported by the BMBF, Bonn under contract no. 05 H11PEA/6. Çiğdem İşsever thanks the Studienstiftung des Deutschen Volkes for a fellowship and the University of Dortmund for a special research position. Kerstin Borras was supported by a Lise Meitner-fellowship of the MWF, Düsseldorf.

References

[1] J. Engler, et al., Nucl. Instr. and Meth. 106 (1973) 189.
[2] V. Böhmer, et al., Nucl. Instr. and Meth. 122 (1974) 313.
[3] J. Moritz, et al., KfK-Report 1936, 1974.
[4] M. Holder, et al., Nucl. Instr. and Meth. 151 (1978) 69;
H. Abramowicz, et al., Nucl. Instr. and Meth. 180 (1981) 429.
[5] R. Wigmans, Nucl. Instr. and Meth. A 259 (1987) 389.
[6] T.A. Gabriel, et al., IEEE Trans. Nucl. Sci. NS-32 (1985) 697;
M.S. Goodman, T.A. Gabriel, A. Di Ciaccio, R. Wilson, Nucl. Instr. and Meth A 278 (1989) 441;
J.E. Brau, T.A. Gabriel, Nucl. Instr. and Meth. A 275 (1989) 190.
[7] H. Brückmann, U. Behrens, B. Anders, Nucl. Instr. and Meth. A 263 (1988) 136.
[8] ZEUS Collaboration, Nucl. Instr. and Meth. A 290 (1990) 95;
ZEUS Collaboration, Nucl. Instr. and Meth. A 289 (1990) 115;
ZEUS Collaboration, Nucl. Instr. and Meth. A 309 (1991) 101.
[9] WA78 Collaboration, Nucl. Instr. and Meth. A 243 (1986) 138;
WA78 Collaboration, Nucl. Instr. and Meth. A 248 (1986) 326.
[10] H1 Collaboration, Nucl. Instr. and Meth. A 336 (1993) 499.
[11] H1 Collaboration, Nucl. Instr. and Meth. A 250 (1994) 57.
[12] H1 Collaboration, Nucl. Instr. and Meth. A 275 (1989) 246;
H1 Collaboration, Nucl. Instr. and Meth. A 265 (1988) 419.
[13] H1 Collaboration, DESY 89-022, 1989.
[14] L. Görlich, H.P. Wellisch, H1 Internal Report H1-12/91-204, 1991.
[15] H1 Collaboration, Nucl. Instr. and Meth. A 344 (1994) 492.
[16] H.P. Wellisch, J.P. Kubenka, H. Oberlack, P. Schacht, MPI-PhE/94-03, 1994.
[17] V. Shekelyan, H1 Internal Report H1-04/93-288, 1993.
[18] J. Gayler, H. Küster, P. Loch, H1 Internal Report H1-04/91-171, 1991.
[19] W. Hofmann, et al., Nucl. Instr. and Meth. 135 (1976) 151.
[20] G. Jaffe, Ann. Phys. 42 (4) (1913) 307;
H.A. Kramers, Physica XVIII (1952) 665.
[21] H1 Calorimeter Group, DESY-01-188, Nucl. Instr. and Meth. A 490 (2002) 204.
[22] M. Korn, Untersuchungen zur Messung der Energie von Elektronen und geladenen Pionen mit dem Flüssigargon-Kalorimeter des Detektors H1, Ph.D. Thesis, Dortmund, 1994.
[23] H1 Calorimeter Group, Nucl. Instr. and Meth. A 350 (1994) 57.
[24] H1 Collaboration, Nucl. Instr. and Meth. A 386 (1996) 348.
[25] H1SIM, H1 software package to simulate particle interaction in the H1 detector.
[26] ARCET, H1 software package to simulate particle interactions in the H1 test setup.
[27] R. Brun, et al., CERN-DD/EE84-1, 1987.
[28] H. Fesefeldt, PITHA 85/02, Aachen, 1985.
[29] T.A. Gabriel, W. Schmidt, Nucl. Instr. and Meth. 134 (1976) 271.
[30] Ç. İşsever, Entwicklung eines alternativen Gewichtungsverfahrens für das H1-Kalorimeter, Diplomarbeit Dortmund 1996, DESY Internal Report FH1-96-06, August 1996.
[31] W. Hofmann, et al., Nucl. Instr. and Meth. 195 (1982) 475.
[32] J. Marks, private communication, 2001.
[33] C. Schwanenberger, The Jet Calibration in the H1 Liquid Argon Calorimeter, Prepared for 10th International Conference on Calorimetry in High Energy Physics (CALOR 2002), Pasadena, CA, 25–30 March 2002; Published in Calorimetry in Particle Physics, Pasadena, 2002, pp. 761–766, physics/0209026.
[34] V. Morgunov, Calorimetry Design with Energy-Flow Concept, Prepared for 10th International Conference on Calorimetry in High Energy Physics (CALOR 2002), Pasadena, California, 25–30 March 2002; Published in Calorimetry in Particle Physics, Pasadena, 2002, pp. 70–84.